Modeling and Validation of Grid-to-Vehicle (G2V) and Vehicle-to-Grid (V2G) Operation with Combo CCS Type 2 Connector for Medium Duty Electric Vehicle Applications

Shahid Jaman[1,2], Oscar Hernandez Garcia[3], Mohamed Abdel-Monem[3], Thomas Geury[1,2] and Omar Hegazy[1,2*]
[1]MOBI-EPOWERS Research Group, ETEC Department, Vrije Universiteit Brussel (VUB), Pleinlaan 2, 1050 Brussel.
[2]Flanders Make, Gaston Geenslaan 8, 3001 Heverlee, Belgium.
[3]Products Innovation & Systems Verification (PI&SV) team, Powerdale (PWD), Witte Patersstraat 4, 1040 Brussel, Belgium.
*Correspondence: omar.hegazy@vub.be

Acknowledgements

This work is a part of the eCharge4Drivers project. This project has received funding from the European Union Horizon 2020 research and innovation program under grant agreement No 875131. This content reflects only the authors view and the European Commission is not responsible for any use that may be made of the information this publication contains. This work was also supported by the Flanders-funded ICON project (OPTIBIDS project). Authors also acknowledge Flanders Make for the support to our research group.

Keywords

Grid-to-Vehicle (G2V), Vehicle-to-Grid (V2G), Combo CCS Type 2 Connector, Modeling, Validation, Medium-Duty Electric Vehicles.

Abstract

In this research work, a modeling and control technique for a two-stage DC charger module is described with relevant dynamic equations and transfer functions. The simulation study and real-time testing of charging (G2V) and discharging (V2G) operation for a medium-duty electric vehicle with Combo CCS type 2 connector port is also performed. It is investigated that the power transfer efficiency for V2G operation using the Combo CCS Type 2 connector reaches approximately 94% for 4.8kW and 83% for 3kW. It is also found that higher power charging and V2G operations shows lower Total Harmonic Distortion (THD). For instance, during a power transfer of 5.1kW back to the grid at 60% State of Charge (SoC), the current THD is observed to be 3.12%. In contrast, the THD during charging mode is measured at 2.42%. These results highlight the improved quality of power during high-power charging and V2G operations, indicating reduced harmonic content and enhanced grid stability.

1. Introduction

The trend towards electric vehicles (EVs) is becoming increasingly prevalent as the market for EVs matures and more EVs are made available for commercial sale, indicating that there will likely be a significant increase in their adoption beyond 2025 [1]. It is expected that 2000 electric buses [2], and 200.000 electric vans [3,4] (based on the ratio of expected EVs in Europe and in Belgium) will drive around in Belgium by 2030. According to a predicted scenario presented by McKinsey [5], the EU region would need to install 3.4 million public chargers by 2030 to meet the needs of its future EV fleet. This number includes 2.9 million public chargers for passenger cars, 0.4 million for light commercial vehicles, and 0.1 million for trucks and buses. This would mean that for Belgium 10.000 charging points are required for vans and 1700 for electric buses. Most of these charging points for medium-duty electric vans are designed to accommodate as well light duty EVs which indicates Level 2 chargers are the most feasible solution for 10.000 charging points. These chargers can fully charge an average electric van in approximately 8-10 hours, whereas the DC fast chargers, which typically have a power output ranging from 50 kW to 350 kW, can charge the battery up to 80 percent of state-of-charge (SoC) in around 10 minutes. Thus, there is a good prospect on research and development of DC chargers for medium duty electric vehicle applications.

On the other hand, most European EV manufacturers are adjusting or modifying their EV models to enable successful bidirectional power flow. If 50% of the predicted charging points for medium-duty EVs are capable of transferring 15kW of power back to the grid, approximately 75MW of power can be supplied to the public power grid during periods of high public load demand. However, the power flow from vehicle to grid requires a compatible connector port with suitable communication protocol. Currently, V2G technology is only commercially feasible using CHAdeMO DC chargers with the associated communication protocol, meaning that only vehicles equipped with CHAdeMO, such as Nissan and Mitsubishi, can be used to benefit

from the V2G functionality [6]. However, Europe are developing their charging infrastructure for the Combined Charging System (CCS) Type 2 connector for AC and DC charging, along with the ISO 15118.20 communication protocol. As a result, research on charging and V2G testing with the Combo CCS Type 2 connector port has a significant potential for future developments. To sum up, the charging power quality and V2G information for medium duty electric vehicles is not available in the market which is the main contribution of this work. Moreover, the ISO15118.20 communication validation is also a challenge to perform V2G in medium duty electric vehicles. this paper, a two-stage DC charger module modeling and control is studied with necessary mathematical equations which represents the real test setup. Moreover, the charging (Grid-to-vehicle, G2V) and discharging (Vehicle-to-Grid, V2G) are tested in the lab with combo CCS type 2 port for medium duty electric vans as shown in Fig. 1. The AC and DC signals performance from simulation and test bed are analyzed with efficiency and THD levels for charging and V2G operation.

2. Bidirectional Two-stage Converter Modeling and Control

The two-stage converter is modelled with state-space equations, represented by matrices A, B,

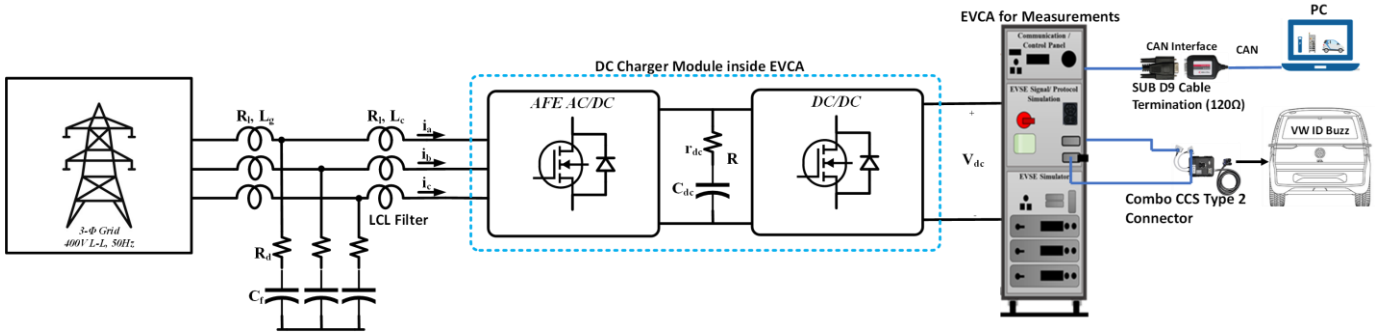

Fig.1: Block diagram of Charging and V2G testing architecture with necessary communication device for medium-duty electric vehicles.

C, and D, which are obtained after solving the first-order differential equations of the LCL filter. A DC filter is considered for the 2-level three-phase AC/DC converter in the *dq* axis [7]-[11]. The equations comprise the grid-side voltage equations (Eq (1)-Eq (2)), filter capacitor current equations (Eq (3)-Eq (4)), converter side voltage equations (Eq (5)-Eq (6)) and dc-link current equation Eq (7). L_g and L_c are the filter inductances of the grid and converter side with resistance R_l. The filter capacitor with damping resistance is expressed as C_f and R_d respectively. The dq components of current (i_{dq}) and voltage (V_{dq}) are obtained via Park transformation with grid frequency (f). The closed-loop transfer function of the AC/DC module is obtained from the state-space model using MATLAB/Simulink.

$$V_{gd} = R_l i_{gd} + R_d i_{gd} + L_g \frac{di_{gd}}{dt} - \omega L_g i_{gq} + V_{fd} - R_d i_{cd} \quad (1)$$

$$V_{gq} = R_l i_{gq} + R_d i_{gq} + L_g \frac{di_{gq}}{dt} + \omega L_g i_{gd} + V_{fq} - R_d i_{cq} \quad (2)$$

$$0 = -i_{gd} + C_f \frac{dV_{fd}}{dt} - \omega C_f V_{fq} + i_{cd} \quad (3)$$

$$0 = -i_{gq} + C_f \frac{dV_{fq}}{dt} + \omega C_f V_{fd} + i_{cq} \quad (4)$$

$$-V_{cd} = R_l i_{cd} + R_d i_{gd} + L_c \frac{di_{cd}}{dt} - \omega L_c i_{cq} + V_{fd} - R_d i_{gd} \quad (5)$$

$$-V_{cq} = R_l i_{cq} + R_d i_{gq} + L_c \frac{di_{cq}}{dt} + \omega L_c i_{cd} + V_{fq} - R_d i_{gq} \quad (6)$$

$$C_{dc} \frac{dV_{dc}}{dt} = \frac{3}{2}(2d_d - 1) i_{cd} + \frac{3}{2}(2d_q - 1) i_{cq} + \frac{V_{dc}}{R} \quad (7)$$

$$\frac{dX}{dt} = \dot{X} = [A]^{7x7} X + [B]^{7x4} U \quad (8)$$

$$Y = [C]^{7x7} X + [D]^{7x4} U \quad (9)$$

where, $X = [i_{gd}\ i_{gq}\ V_{fd}\ V_{fq}\ i_{cd}\ i_{cq}\ V_{dc}]^T$ and $U = [V_{cd}\ V_{cq}\ V_{gd}\ V_{gq}]^T$

In the above equations, V_{dc} is output voltage and d_{dq} are the duty cycles in *dq* reference frame. The transfer function $G_{VSC}(s)$ derived from state space model is used as a plant function during control parameters tuning. On the other hand, the three-phase interleaved bidirectional DC/DC converter, as shown in Fig. 2, operates as a buck converter during charging mode when the charging power flows from the DC-link to the battery. The DC-link voltage serves as the input to the converter, while the battery side operates as the output and vice versa.

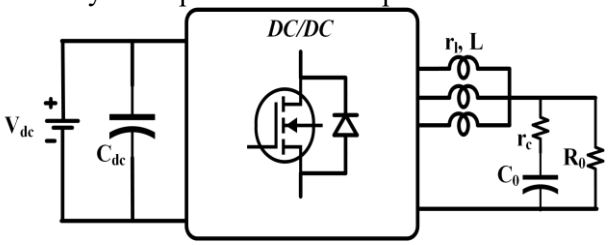

Fig. 2: Bidirectional 3-phase Interleaved DC/DC Converter

During V2G operation, the converter works in boost mode. Let us consider a three-phase interleaved DC/DC converter that has an interleaved inductance L with internal resistance r_l, and output capacitor C_0 with resistance r_c. The load resistance is R_0. The current control loop plant transfer function is obtained based on the small-signal model of G2V and V2G operation, which is expressed in Eq (10)-Eq (11) [12]-[14].

$$G_{id_{buck}}(s) = \frac{i_L(s)}{d(s)} = \frac{V_0}{DL} \frac{s + \frac{1}{R_0 + r_c}}{s^2 + 2P_1 P_2 s + P_2^2} \quad (10)$$

where,

$$P_1 = \frac{C_o(r_l R_o + r_l r_c + R_o r_c)}{2\sqrt{LC_o(R_o + r_c)(r_l + R_o)}}$$

$$P_2 = \sqrt{\frac{r_l + R_o}{LC_o(R_o + r_c)}}$$

$$G_{id_{boost}}(s) = \frac{i_L(s)}{d(s)} = \frac{V_o}{r_l + 3(1-D)^2 R_o} \frac{s + \frac{1}{C_o(R_o + r_c)}}{s^2 + 2P_1P_2s + P_2^2} \quad (11)$$

where,

$$P_1 = \frac{L + C_o[r_l R_o + r_l r_c + 3(1-D)^2 R_o r_c]}{2\sqrt{LC_o(R_o + r_c)[r_l + 3(1-D)^2 R_o]}}$$

$$P_2 = \sqrt{\frac{r_l + 3r_c R_o(1-D)^2}{2LC_o(R_o + r_c)}}$$

Similarly, the voltage control loop plant transfer function is obtained based on the small-signal model of G2V and V2G operation, which is expressed in Eq (12)-Eq (13).

$$G_{vd_{buck}}(s) = \frac{v_{bat}(s)}{d(s)} = \frac{V_o R_o r_c}{3D(R_o + r_c)} \frac{s + \frac{1}{C_o r_c}}{s^2 + 2P_1P_2s + P_2^2} \quad (12)$$

where,

$$P_1 = \sqrt{\frac{r_l + R_o}{LC_o(R_o + r_c)}}$$

$$P_2 = \frac{C_o(r_l R_o + r_l r_c + R_o r_c)}{2\sqrt{LC_o(R_o + r_c)(r_l + R_o)}}$$

$$G_{vd_{boost}}(s) = \frac{i_L(s)}{d(s)} = \frac{V_o r_c}{(1-D)(R_o + r_c)} \frac{\left(s + \frac{1}{C_o r_c}\right)\left(s + \frac{3(1-D)^2 R_o - r_l}{L}\right)}{s^2 + 2P_1P_2s + P_2^2} \quad (13)$$

where,

$$P_1 = \frac{L + C_o[r_l R_o + r_l r_c + 3(1-D)^2 R_o r_c]}{2\sqrt{LC_o(R_o + r_c)[r_l + 3(1-D)^2 R_o]}}$$

$$P_2 = \sqrt{\frac{r_l + 3r_c R_o(1-D)^2}{2LC_o(R_o + r_c)}}$$

The detailed of the control design with the dual loop control gains estimation strategy is discussed in [12]. The control of the AC/DC converter consists of an outer loop for DC bus voltage control and an inner loop current control. In case of grid current control shown in Fig. 3(a), the desired grid current reference is compared to the measured and filtered actual one. The PI controller has been chosen thanks to its robustness, flexible implementation, and easy design [15]. In case of dc-link voltage control, the dc-link voltage reference signal is compared to the measured and filtered actual DC-Bus voltage as shown in in Fig. 3(b), and the PI controller ensures that the output signal remains within a certain range to avoid system saturation. The controller used is digital and modeled according to the characteristics of the grid current control. After offline control design, this control strategy is integrated into the non-linear simulation model of MATLAB/Simulink. The controller generates signals for the six switches of the AC/DC converter's two-level topology.

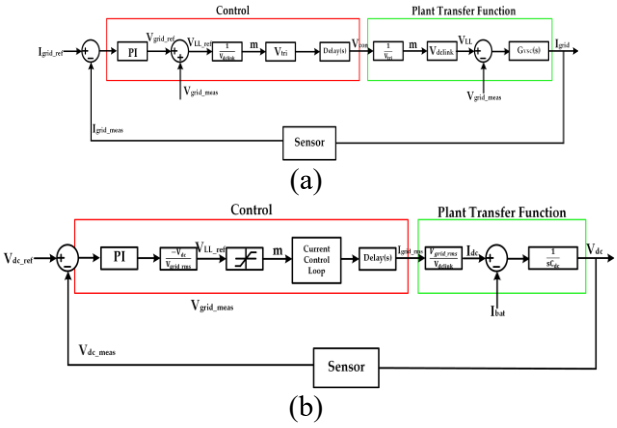

Fig. 3 Control block diagrams for the bidirectional AC/DC Converter. (a). Grid current control. (b). DC-link voltage control.

The DC/DC converter operates differently based on the direction of power flow. During G2V operation a digital PI controller generates the battery side inductor's voltage by comparing a certain battery current reference to the measured and filtered actual current as shown in Fig. 4. During charging mode, the battery voltage is added to obtain the duty cycle, d for the MOSFET switching, which compensates for the battery voltage (V_{bat}) introduced in the system, leading to better response and tracking of the battery current, I_{bat}.

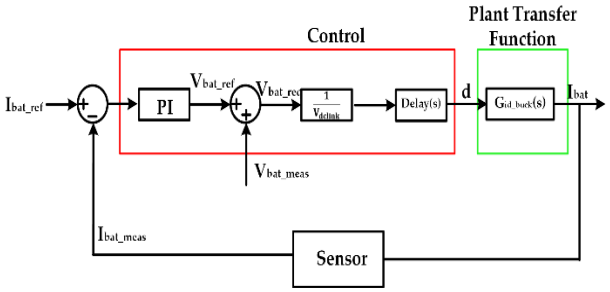

Fig. 4 Battery current control of bidirectional DC/DC converter in charging mode

Alternatively, during V2G mode operation [15], the plant system incorporates Vbat, which entails dividing the battery voltage by the DC-Bus voltage to derive 1-d , where d represents the control signal depicted in Fig. 5. This signal is used to switching the MOSFET after processing to duty cycle. d.

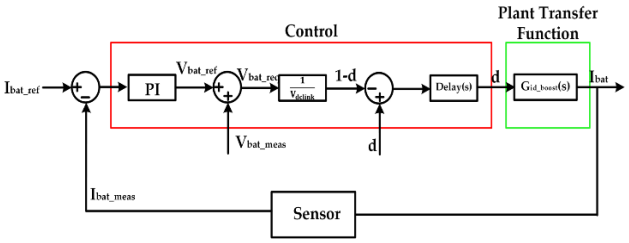

Fig. 5 Battery current control of bidirectional DC/DC converter for V2G operation

3. Overall Test System Description

This paper considers a DC charging test system that incorporates the Combo CCS type 2 charging port standard during V2G testing. The medium duty Volkswagen ID Buzz electric van is used as the vehicle

under test with necessary hardware and software modifications. The charging test uses an Electric Vehicle Charging Analyzer (EVCA), which has been tested to ensure safe operation in accordance with current standards and charger interfaces. The system uses the necessary equipment to measure and verify communication, protection, safety, and load circuit conformity over the entire charging duration and captures any deviations. This helps to identify charging non-conformity and reasons for charge interruptions.

3.1. Electric Vehicle Charging Analyzer (EVCA)

The EVCA is a device capable of monitoring both the load and communication circuit throughout the entire electric vehicle charging process. By identifying and logging any variances from established standards, it facilitates the evaluation of conformity with all pertinent parameters while analyzing measurement files. The data generated can be sent to external equipment for further processing through the CAN communication protocol. The EVCA is versatile enough to test various charger types, including both AC and DC chargers. It operates in three distinct modes: 1) EV emulator, 2) EVSE emulator for AC and DC chargers, and 3) Man-in-the-middle. This unit is designed for testing and analyzing the conductive charging-discharging of EVs. In this test, the integrated DC charger module with EVCA is considered.

3.2. Medium Duty Electric Van (Volkswagen ID Buzz)

The Volkswagen ID. Buzz is an electric minivan which is shown in Fig. 6 produced by Volkswagen, based on the MEB platform. It is the first electric minivan from Volkswagen and part of the ID. series. The ID. Buzz's design is inspired by the Volkswagen Type 2 (T1) Microbus.

(a)

(b)

Fig.6. (a)Volkswagen ID. Buzz electric van with new driving range. (b)Combo CCS type 2 connector port for AC and DC charging.

The battery type is Lithium-ion with a nominal capacity of 82 kWh (usable 77 kWh) and a pack nominal voltage of 350V [16]. Moreover, this vehicle supports both home charging and fast charging. The AC charging port (type 2) with 11kW is compatible during home/slow charging. On the other hand, VW ID buzz can also be charged with fast charger (175 kW max) with combo CCS port. The charging duration is 8 hours and around 30 min for slow and fast charging respectively. Since, the V2G specifications with Combo CCS Type 2 connector technology is still under development, the V2G information for this medium duty vehicle is not provided in the vehicle's specification. In this work, the V2G performance assessment with power quality is the focus for electric van.

4. Simulation Model Results

The control loop performance shows that the inner current loop operates slightly faster than the outer voltage loop in both converters, while both are operating in a stable region as confirmed by the Bode plot. The frequency responses of the current and voltage control feedback loops of the AC/DC converter are depicted in Fig. 7 and Fig. 8, indicating that the faster inner current loop maintain stability with a gain margin of 30.7dB and a phase margin of 120° until the converter side inductance (L_c) increased 200 times from the based designed value. Similar way, the slower outer voltage control loop attains stability with a gain margin of 85dB and a phase margin of 120°.

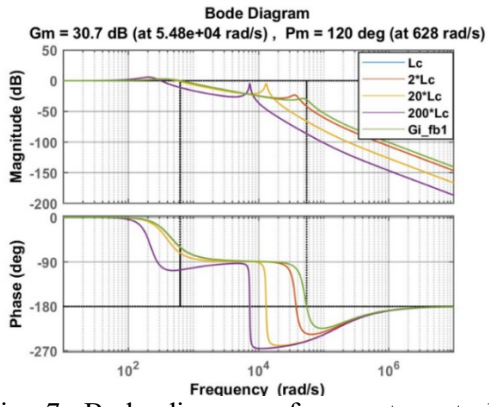

Fig. 7: Bode diagram of current control loop of AC/DC converter in different converter side inductance value.

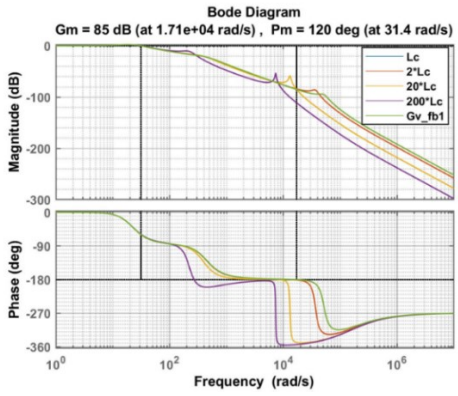

Fig. 8: Bode diagram of voltage control loop of AC/DC converter in different converter side inductance value.

The design parameters and specifications that have been considered in this work are shown in Table I and then discussed.

Table I: System specification and designed parameters

Parameters	Value	Parameters	Value
Battery capacity	77KWh	Filter Inductance (Grid Side). L_g	0.813mH
Output Power	30KW	Filter Capacitance. C_f	30uF
Battery Nominal Voltage	340V	Filter Inductance (Converter Side), L_c	0.867mH
Rated Capacity	50Ah	ESR+Damping resistance, R_d	10 Ω
Rated AC Input Voltage, frequency	380V, 50Hz	Output filter Inductance, L_0	0.0125m H
Max. Charge/discharge current at 1C	50A	Output Filter Capacitance, C_0	1000uF
Switching frequency, f_{sw}	10kHz		

The simulation study is conducted for charging and V2G up to 11kW with 0.6 C-rate. The current reference is changed with 5A step. The battery is charged up to t=1.25sec with CC and CV mode. During this charging, the current setpoint changes from 20A at 0.75sec to 30A at 1.25sec, as shown in Fig. 9(a). The nominal voltage is 340V with 50Ah capacity. The discharging current profile is also shown in Fig. 9(a). The battery voltage responds to the power demand for both modes as shown in Fig. 9(b).

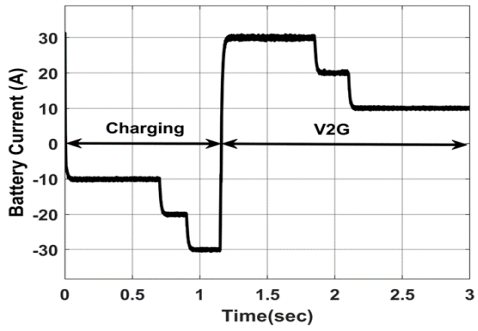

(a)

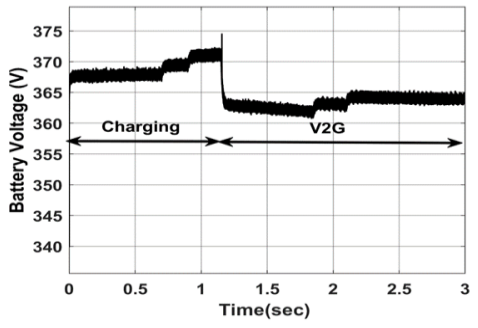

(b)

Fig. 9. The battery current and voltage performance during 11kW charging and V2G operation. (a) battery current profile. (b). battery voltage profile

Moreover, the SoC profile variation is shown in Fig. 10(a). It is observed that the SoC is increased around 2% from the initial state within 1.2 sec by drawing charging current up to 0.6C (30A). Moreover, the SoC decreased by 4% by discharging up to 30A (0.6C) with 1.8 sec. The battery power profile with an 11kW (0.6C) transfer to the grid is shown in Fig. 10(b). On the other hand, the dc-link voltage controller is maintaining the 750V setpoint with a 10-15V voltage ripple, as shown in Fig. 10(c). During the transition mode, the voltage ripple is 100V which is not a problem for high power semiconductor switches.

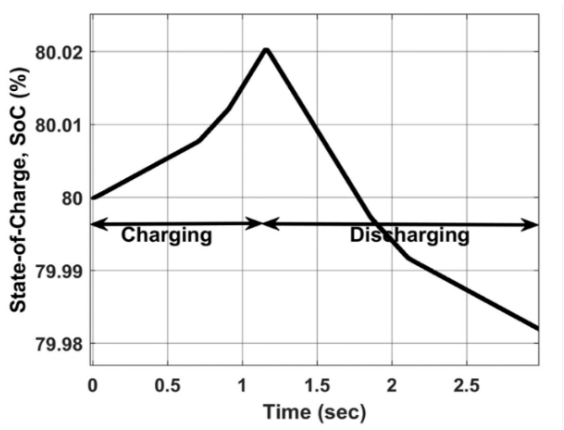

(a)

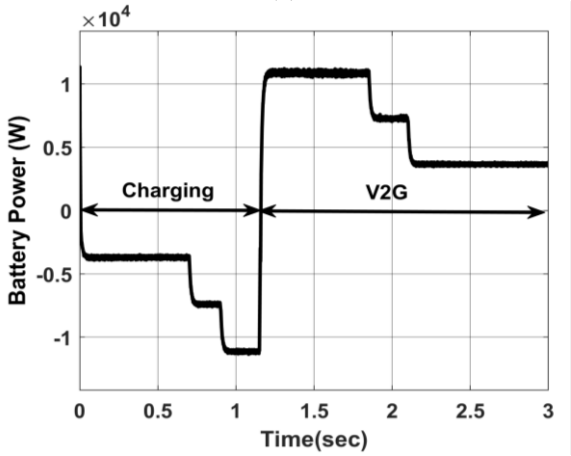

(b)

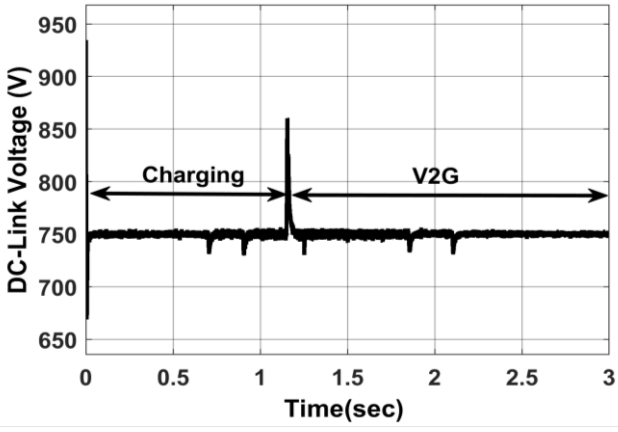

(c)

Fig. 10. The battery (a) SoC profile, (b) bidirectional power flow, and (c) DC-link voltage profile during 11kW charging and V2G operation.

5. Charging and V2G Test Results

The real-time testbed setup with VW ID Buzz is shown in Fig. 11. To set up the EV Charging Analyzer (EVCA) with integrated DC charger module, connect it to the battery voltage and current are shown in Fig. 12. The operator specifies the charging and discharge current setpoints. Initially, the charging current is set to 5A, and then it is increased up to 15A. The battery voltage starts from around 360V to increase during charging. Conversely, the discharging setpoints increased from -5A to -15A. The battery voltage decreased to 340V during 0.6C discharge. The rated power of the DC charger module is 15kW.

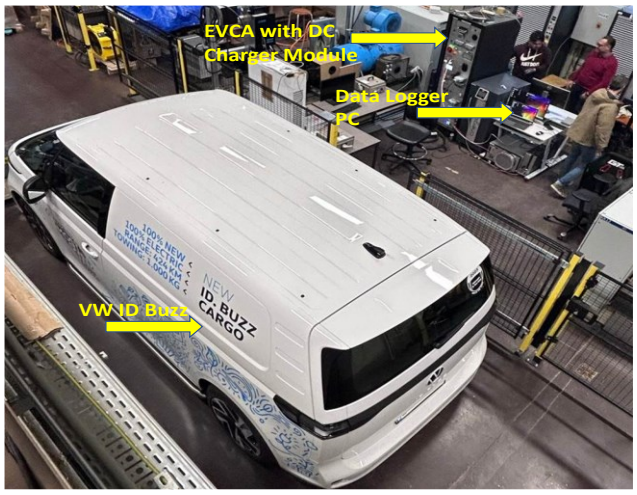

Fig. 11: The laboratory test system setup for charging and V2G for VW ID Buzz.

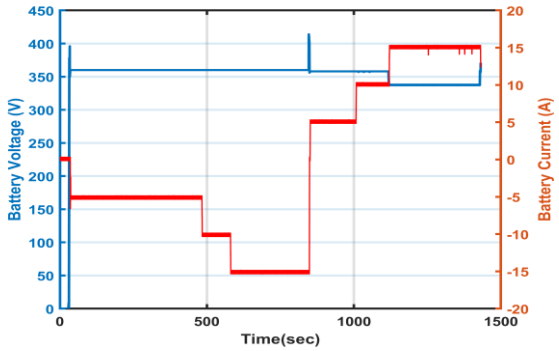

Fig. 12: Battery voltage and current data EVCA measurement.

The simulated current and voltage waveforms from the AC side are shown in Fig. 13, which depicts the charging and discharging modes with transition phenomena. It is shown that around 42A rms grid current flows to the DC charger to transfer the 11kW charging power. However, around 20A rms current flows to the grid from EVSE during same amount of power request. The transition happens at t=1.15sec. On the other hand, in real-time testing, 3kW power is transferred to the grid after the transition phenomena. It is also observed that the AC voltage is around 233V (phase) and is in phase opposition with the grid current. The charger transfers 4.8kW to the grid when the DC power supplied to the battery is 5.1kW. Similarly, 3kW is transferred back to the grid when the battery supplies 3.55kW DC power. The signal waveform is shown in Fig. 14.

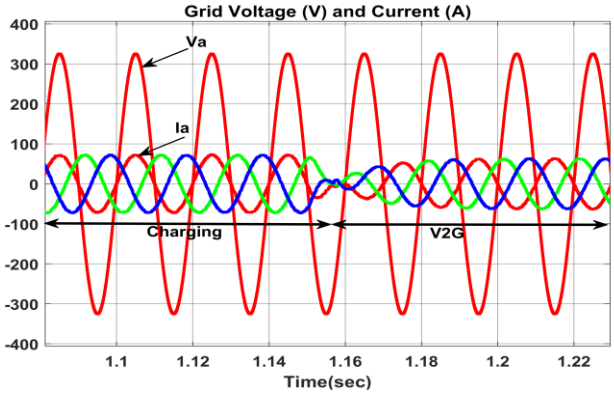

Fig. 13: The current and voltage waveform of charging to V2G operation from simulation model.

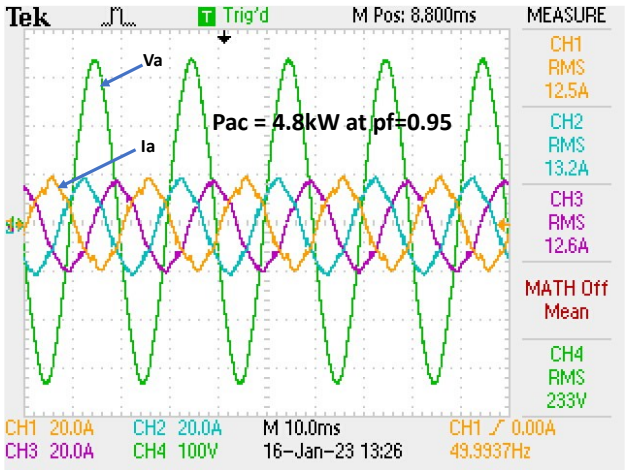

(a)

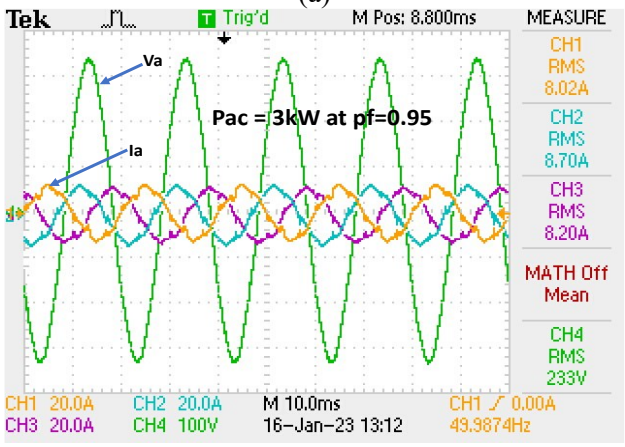

(b)

Fig. 14: Phase voltage and current waveforms during power transfer back to the grid (V2G) through Combo CCS Type 2 port. (a) 4.8 kW transfer, (b). 3 kW transfer to the grid.

The charging and V2G efficiencies are estimated for DC charger module at 3 different SoC levels. Since the charger module is 15kW and the maximum tested power 5.1kW, the converter is led to its maximum efficiency. The efficiency curve for charging and V2G is shown in Fig. 16; around 94% V2G efficiency is possible with this charger module when 5.1kW power is fed back to the grid whereas 96% efficiency is estimated during charging at same power level. The

efficiency is lower at low power transfer in both directions.

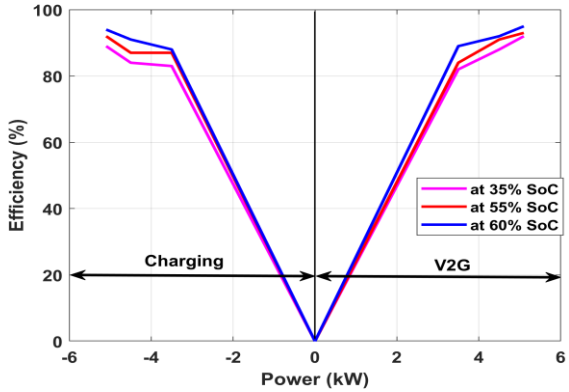

Fig. 16: Tested charging and V2G efficiency up to 6kW for VW ID Buzz at different SoC profiles.

The THD level of the charging and discharging currents are also estimated using FFT analysis from simulation model. During the test, it is noticed that the THD is very high at 20% of rated power. The current waveform starts good THD when the power transfers the charger is 45%-50% of the rated power. The THD of different power levels is shown in Table II below:

Table II: THD levels during Charging and V2G operation at 3 different initial SoC levels.

	35%SoC	55%SoC	60%SoC
Charging			
-3500W	6.34%	5.87%	5.19%
-4500W	4.29%	3.92%	3.46%
-5100W	3.26%	2.81%	2.42%
V2G			
3500W	8.12%	6.23%	5.78%
4500W	7.51%	5.24%	4.38%
5100W	6.85%	4.25%	3.12%

Moreover, the THD is high during V2G operation compared to charging which is greater than 5% for 50% initial SoC. The THD is high during V2G because the electric vehicle's charger introduces additional harmonics into the grid when they operate in reverse power mode to supply power to the grid. This happens because the charger is designed to operate in a specific range and supplying power to the grid may cause the equipment to operate outside its normal range, resulting in harmonic distortion. Additionally, the load on the grid during V2G operation is variable and unpredictable, and this can cause voltage fluctuations and increase the THD. The voltage fluctuations can result in non-linear behavior of the grid, leading to additional harmonic distortion. To reduce THD during V2G, grid operators can implement advanced power electronics that are designed to operate in V2G mode and can filter out harmonic components. Furthermore, implementing power quality monitoring and control systems can help manage the variability and unpredictability of the load on the grid and reduce THD.

6. Conclusion

In this paper, a dynamic equation-based two-stage converter modeling and control approach for charging and V2G operation is described. For the simulation study, up to ±30A current is requested to the battery with 340V nominal voltage and around 11kW of requested power. The real-time test is performed with the same charging and discharging profiles up to ±6kW for VW ID Buzz. The Combo CCS type 2 connector port is used during the test. It is noticed that the battery voltage profile variation is almost matched with simulated profile. The 4.8kW and 3kW power is successfully transferred back to the grid via Combo CCS port with around 94% and 83% efficiency, respectively. However, the efficiency curve variation is noticeable considering different initial SoC levels. Moreover, the THD is lower at high power charging and V2G operation. It is observed that the current THD is 3.12% with 5.1kW power transferred back to the grid at 60% SoC whereas it shows 2.42% THD during charging mode.

References

[1] Frost and Sullivan "European medium-duty and high-duty electric trucks growth opportunities" Global Information, Dec 24, 2021. Available on https://www.giiresearch.com/report/fs1053948-european-medium-duty-heavy-duty-electric-trucks.html [accessed on 28 Feb, 2023]

[2] "Brussles transit company STIB will replace 411 diesel buses by 2030" Brussels Times, 23 Apr, 2023. Available on https://www.brusselstimes.com/219102/brussels-transit-company-stib-will-replace-411-diesel-buses-by-2030 [accessed on 28 Feb, 2023]

[3] "De Lijn to buy up to 1,250 electric buses within 6 years"Available on https://www.electrive.com/2022/03/31/de-lijn-to-procure-up-to-1250-electric-buses-within-six-years/ [accessed on 28 Feb, 2023]

[4] Max Molliere "E-Vans: Cheaper, Greener andin demand" Transport Environment, March 2022. Available on https://www.transportenvironment.org/wp-content/uploads/2022/03/2022_03_van_TCO_report-1.pdf [accessed on 28 Feb, 2023]

[5] Julian Conzade, Florian Nägele, Swarna Ramanathan, and Patrick Schaufuss "Europe's EV opportunity—and the charging infrastructure needed to meet it" Mckinsey & Company, Nov 2022. Available on https://www.mckinsey.com/industries/automotive-and-assembly/our-insights/europes-ev-opportunity-and-the-charging-infrastructure-needed-to-meet-it [accessed on 28 Feb 2023]

[6]. "Industry Learning Reports." Available online: https://www.v2g-hub.com/reports (accessed 28 Feb 2023)

[7] W. Qiang, L. Yong-bao, H. Xing, and L. Qian-chao, "Simulation Study of Three-phase PWM Rectifier with Square of the Voltage Double Closed Loop Control," in IOP Conference Series: Materials Science and Engineering, 2017, vol. 199, no. 1, p. 12148.

[8] W. U. XINHUI, "Analysis, design and implementation of

high performance control schemes for three phase PWM AC-DC voltage source converter." 2008.

[9] P. Ruttanee, K. N. Areerak, and K. L. Areerak, "Averaging Model of a Three-Phase Controlled Rectifier Feeding an Uncontrolled Buck Converter," World Acad. Sci. Eng. Technol. J., vol. 60, pp. 345–352, 2011.

[10] K. Chaijarurnudomrung, K. N. Areerak, and K. L. Areerak, "Modeling of three-phase controlled rectifier using a DQ method," in 2010 International Conference on Advances in Energy Engineering, 2010, pp. 56–59.

[11] S. Chakraborty, H. Rasool, D. -D. Tran, T. Geury, M. E. Baghdadi and O. Hegazy, "Design and Implementation of a Multifunctional 6-phase Interleaved Bidirectional DC/DC Converter for Battery Electric Vehicle Applications," 2021 23rd European Conference on Power Electronics and Applications (EPE'21 ECCE Europe), Ghent, Belgium, 2021, pp. 1-10.

[12]. S. Jaman, S. Chakraborty, M. E. Baghdadi, T. Geury and O. Hegazy, "Small-Signal Average Switch Modeling and Dual-Loop Control of Bidirectional Integrated Converter for G2V and V2G Applications in Battery EVs," 2021 23rd European Conference on Power Electronics and Applications (EPE'21 ECCE Europe), Ghent, Belgium, 2021, pp. 1-12.

[13]. O. Hegazy, J. V. Mierlo and P. Lataire, "Analysis, Modeling, and Implementation of a Multidevice Interleaved DC/DC Converter for Fuel Cell Hybrid Electric Vehicles," in IEEE Transactions on Power Electronics, vol. 27, no. 11, pp. 4445-4458, Nov. 2012.

[14]. S. Chakraborty, D. -D. Tran, J. van Mierlo and O. Hegazy, "Generalized Small-Signal Averaged Switch Model Analysis of a WBG-based Interleaved DC/DC Buck Converter for Electric Vehicle Drivetrains," 2020 22nd European Conference on Power Electronics and Applications (EPE'20 ECCE Europe), Lyon, France, 2020, pp. P.1-p.8.

[15]. Garcés Quílez, M.; Abdel-Monem, M.; El Baghdadi, M.; Yang, Y.; Van Mierlo, J.; Hegazy, O. Modelling, Analysis and Performance Evaluation of Power Conversion Unit in G2V/V2G Application—A Review. Energies 2018, 11, 1082

[16]. Electric Vehicle Database "Volkswagen ID Buzz". Available on https://ev-database.org/car/1651/Volkswagen-ID-Buzz-Pro [accessed on 28 Feb, 2023]